Published in final edited form as:

Nat Struct Mol Biol. 2009 September ; 16(9): 930–937. doi:10.1038/nsmb.1649.

The molecular basis for the regulation of the CBC by the importins

Sandra M.G. Dias[1], **Kristin F. Wilson**[1], **Katherine S. Rojas**[1], **Andre L.B. Ambrosio**[1], and **Richard A. Cerione**[1,2]

[1]Department of Molecular Medicine, College of Veterinary Medicine, Cornell University, Ithaca, New York. 14853, USA

[2]Department of Chemistry and Chemical Biology, Baker Laboratory, Cornell University, Ithaca, New York. 14853, USA

Abstract

The binding of capped RNAs to the cap-binding complex (CBC) in the nucleus, and their dissociation from the CBC in the cytosol, represent essential steps in RNA-processing. Here we show how the nucleocytoplasmic transport proteins, importin-α and importin-β, play key roles in regulating these events. As a first step toward understanding the molecular basis for this regulation, we determined a 2.2 Å resolution x-ray structure for a CBC-importin-α complex that provides a detailed picture for how importin-α binds to the CBP80 subunit of the CBC. Through a combination of biochemical studies, x-ray crystallographic information, and small-angle scattering experiments, we then determined how importin-β binds to the CBC through its CBP20 subunit. Together, these studies enable us to propose a model describing how importin-β stimulates the dissociation of capped RNA from the CBC in the cytosol following its nuclear export.

INTRODUCTION

Eukaryotic RNA polymerase II transcripts (mRNAs and U snRNAs) are modified by the addition of a 7-methyl guanosine cap ($m^7G(5')ppp(5')N$) through a 5'-5' triphosphate linkage. The cap serves as a recognition site for the cytosolic protein eIF4E which plays an essential role in cap-dependent mRNA translation1, and for the nuclear cap-binding complex (CBC) which regulates the splicing efficiency of cap-proximal introns2, stimulates 3'-end formation2 as well as the export of U snRNAs and mRNAs2,3, and mediates a pioneer round of translation for mRNAs subject to nonsense-mediated decay4-6. The CBC is comprised of a 20 kDa cap-binding subunit, CBP20, and an 80 kDa regulatory subunit,

Correspondence should be addressed to R.A.C. rac1@cornell.edu.

AUTHOR CONTRIBUTIONS S.M.D. designed and performed the protein purifications, EMSA, crystallography, UV-crosslinking assays, pull-downs, native gels, SAXS, bioinformatics work and AUC experiments, analyzed data, and wrote the paper; K.F.W. designed and performed cell biology experiments, analyzed data and wrote the paper; K.S.R. performed cell biology experiments; A.L.B.A. analyzed crystallographic data; and R.A.C. analyzed data and wrote the paper.

Accession codes Atomic coordinates and diffraction data were deposited in the Protein Data Bank at www.rcsb.org (PDB codes 3FEY and 3FEX).

CBP80. The roles played by the CBC in RNA processing are mediated through its interactions with a number of proteins. For example, PHAX couples the CBC to CRM1 in the export of U snRNAs7,8, and Aly bridges the CBP80 subunit of the CBC to the mRNA export complex TREX3. Interactions between the CBC and CstF positively affect the cleavage step in 3'-end formation9, and interactions between CBP80 and the poly(A)-specific ribonuclease (PARN) inhibit mRNA deadenylation10. The association of eIF4G1 with CBP80 is necessary for cap-dependent translation in yeast11 and may have a similar function in nonsense-mediated decay in mammalian cells4.

Members of the importin/karyopherin family of nucleocytoplasmic transport proteins also serve as binding partners for the CBC12-16. Importin-α binds to the nuclear localization sequence (NLS) within the N-terminal end of CBP80 and participates with importin-β in the nuclear import of the CBC. The inclusion of importin-α within the cap-binding complex is well conserved from protozoa through eukaryotes14,15 and has been documented through multiple stages of RNA processing16. In addition to their roles in nucleocytoplasmic transport, the importins have also been suggested to regulate the cap-binding activity of the CBC14. While the CBC-importin-α complex binds capped RNA with high affinity, the inclusion of importin-β into this complex appears to stimulate the release of capped RNA14. Likewise, importin-α has been shown to interact with the cap methyltransferase (MT) and enhance its ability to bind and modify its substrate, GpppG-capped RNA, whereas importin-β promotes the dissociation of the MT-RNA-importin-α complex17.

The inter-conversion between the CBC-importin-α and CBC-importin-α-importin-β complexes is regulated by the GTPase Ran, as the interaction between importin-β and GTP-bound Ran18 causes importin-β to dissociate from the CBC-importin-α complex14. Given the high concentrations of Ran-GTP in the nucleus, this provides a mechanism by which the CBC binds capped RNA with high affinity in the nucleus, but with low affinity in the cytosol. The ability of importin-β to trigger the release of capped mRNA from the CBC in the cytosol is a pre-requisite step for the binding of capped mRNA to eIF4E and its translation into protein.

In the present study, we set out to gain a better understanding of how importin-β confers this important regulatory influence. We present a 2.2 Å x-ray crystal structure for the human CBC bound to an importin-α (human) molecule lacking the importin-β-binding domain, that provides a structural picture for how importin-α engages one of its nucleocytoplasmic transport cargo proteins. This and other x-ray crystallographic information, when used in combination with biochemical and mutagenesis studies, small-angle x-ray scattering (SAXS) data, and analytical ultracentrifugation measurements, lead to a mechanistic model for how human importin-β binds to the CBC and stimulates the release of capped RNA. We further validate this model by showing that the binding of the importins to the CBC is essential for the growth factor-regulation of its cap-binding capability.

RESULTS

Structural basis for the binding of the CBC to importin-α

The binding affinity of the CBC for capped RNA was reported to be dependent upon whether the CBC is complexed to importin-α, alone, or together with importin-β14. We re-examined the influence of the importins on the cap-binding capability of the CBC using purified recombinant preparations of these proteins (Supplementary Figs. 1a,b; also see Supplementary Data) and further established that the binding of importin-α, alone, to the CBC does not alter its ability to bind cap, whereas when importin-β binds together with importin-α to the CBC, the affinity for cap is weakened. We therefore wanted to better understand the molecular basis by which the importins influence the cap-binding capability of the CBC.

While x-ray structures have been reported for human importin-α bound to the C-terminal of the viral protein PB2 (ref. 19), and for yeast importin-α bound to peptides representing the monopartite and bipartite NLS motifs20-24, thus far a structural picture of how importin-α engages a full-length nuclear import-cargo protein has not been available. Because the ability of importin-β to bind to the CBC and weaken its binding affinity for cap is influenced by importin-α, we set out to obtain a high-resolution x-ray crystal structure that shows how importin-α binds to the CBP80 subunit of the CBC. To do this, it was necessary to use an importin-α construct that lacked the N-terminal 69 amino acids comprising the importin-β-binding domain (designated importin-αΔIBB). In the presence of cargo, this sequence is most likely disordered21, and indeed crystals were only obtained when it was deleted. The CBC binds importin-αΔIBB as effectively as full-length importin-α, as indicated by their co-elution during gel filtration chromatography (data not shown). Supplementary Fig. 2 shows that the purified CBC-importin-αΔIBB complex contained a stoichiometric amount of the cap-analog, similar to the CBC-importin-α (full-length) complex, as indicated by analytical reverse-phase chromatography.

Two x-ray crystal structures for the human CBC bound to human importin-αΔIBB (isoform importin-α1) were solved to 2.2 Å and 3.5 Å resolution. Only the 2.2 Å resolution structure is presented here (Fig. 1; see Table 1 for statistics). No significant structural changes were observed for the CBP20 and CBP80 subunits complexed to importin-α, when compared to the structures previously reported for the free CBC. Importin-αΔIBB contains an NLS-binding domain consisting of armadillo- (Arm-) repeats containing three α-helices that form a superhelical structure20-24 (Fig. 1). It is now possible for the first time to see the N-terminal 23 residues of CBP80 (Fig. 1, top, shows the electron density map $2F_o-F_c$ for residues 2 to 22), as this region contains the binding site for importin-α13. The N-terminal region of CBP80 has two NLS sequences, i.e. a typical bipartite motif (represented by sticks in Fig. 1, also, see Supplementary Fig. 3a), which bind through extensive contacts to importin-αΔIBB (Supplementary Fig. 3b).

The CBP20 subunit within the CBC-importin-αΔIBB complex conforms to the classical ribonucleotide-binding domain- (RNP-) fold25-27. Although a weak electron density is detected for residues 12–15, the densities for residues 1–11 and 16–29 are not visible, nor for the residues beyond 126. These residues represent additions to the RNP-fold via the N-

terminal (helices α1, α2, and α3) and C-terminal (the β4-αC loop and helix αC) insertions that are involved in binding the cap, thereby enabling the CBC to show functional specificity relative to other RNP-containing proteins26,27. Most of these residues are missing as a consequence of the cap-analog m^7GpppG not being present within the structure.

In light of the results described above, as well as previous work14, we only anticipated release of the cap from the CBC when it was complexed to both importin-α and importin-β, but not when it was bound to importin-α alone. However, an analysis of the crystalline contacts showed that within the location where the cap-analog should be bound to CBP20, there was instead an importin-αΔIBB molecule representing a symmetry partner in the unit cell (Supplementary Fig. 4). The interaction between the importin-αΔIBB symmetry partner and CBP20 includes contacts with Arg112 and Asp114 of CBP20 (Supplementary Fig. 4, inset on the left; also see Supplementary Data). These residues are essential for cap-binding because when each is changed to alanine, the resultant CBC-double mutant binds capped RNA with reduced affinity, as read-out by RNA-gel shift assays (Supplementary Fig. 1a, lane 9). Taken together, these findings suggested that importin-β might also directly engage the CBP20 subunit in order to trigger the release of capped RNA.

Importin-β binds to the CBP20 subunit of the CBC

Attempts to obtain diffracting crystals for the CBC-importin-α-importin-β complex were unsuccessful and so alternative approaches were necessary to investigate how importin-β engages the CBC. We suspected that if importin-β directly binds to the CBP20 subunit to stimulate the release of capped RNA, such an interaction, in the absence of importin-α, would be weak, and indeed we were not able to detect a complex between importin-β and the CBC using standard pull-down assays (data not shown). Therefore, we turned to an agarose native-gel28 and found that importin-β binds to apo-CBC in a dose-dependent manner, as indicated by the serial reduction in the intensity of the band corresponding to free CBC and by the appearance of a band that migrates slightly faster than free importin-β (Fig. 2a, lanes 3 to 8). On a higher pH gel, the complex between the CBC and importin-β yields a very intense band (Fig. 2a, lane 11) compared to the band representing free importin-β (Fig. 2a, lane 10). The addition of the cap-analog m^7GpppG resulted in the emergence of a band corresponding to the CBC no longer bound to importin-β (Fig. 2a, lanes 12–14), consistent with the idea that importin-β binds preferentially to cap-free CBC, and conversely cap-analogs favor binding to the CBC in the absence of importin-β and weaken its affinity for importin-β. Additionally, we found that the CBP20 subunit is capable of directly binding to importin-β. Figure 2b, lanes 1–4, show that the addition of increasing amounts of CBP20 to importin-β resulted in the formation of a complex between these proteins, as indicated by a band on the agarose gel that migrated slower than importin-β alone (under these conditions, free CBP20 did not enter the gel).

We then set out to delineate the region on importin-β necessary for binding to the CBC. Importin-β constructs comprising residues 1–619, 1–445, 45–876, 128–876, and 305–876 were each incubated with the CBC in a 1:1 ratio and then subjected to electrophoresis. The importin-β(45–876) construct was able to form a complex with the CBC as indicated by the lack of a band for free CBC (Fig. 2c, lane 9), whereas the importin-β(128–867) construct

was less effective in binding to the CBC as reflected by the presence of a weak band representing free CBC (Fig. 2c, lane 11). Removal of the N-terminal 305 residues of importin-β completely prevented it from binding to the CBC, again as indicated by the appearance of a diffuse band for free CBC (Fig. 2c, lanes 13). We then showed that importin-β(305–876) lost the ability to promote the dissociation of capped-mRNA from the CBC-importin-α complex and instead formed a super-shifted band as a read-out in RNA gel-shift assays (Fig 2d, lane 5).

How CBP80 and importin-β bind to CBP20 and influence cap-binding

The N- and C-terminal insertions for the RNP-fold of CBP20 are important for cap-binding26,27. The x-ray structure for the CBC bound to the cap-analog m^7GpppG27 shows that the N-terminal α1 and α2 helices from CBP20 fit into a groove within CBP80 (comprised of residues Lys327 and Glu328) (Fig. 3a) that was predicted to be important for stabilizing the α2-α3 loop. This then enables Tyr20 and Tyr43 from CBP20 to participate in π-π stacking interactions required for the high affinity binding of cap26 (also see the structure for full-length CBP20 in Fig. 2b), thus providing an explanation for how CBP80 strengthens the cap-binding capability of the CBP20 subunit. The importance of the C-terminal region of CBP20 in binding the cap is suggested by the finding that when Tyr138 (see structure for full-length CBP20 in Fig. 2b) was changed to alanine, the affinity for m^7GpppG was weakened29. In addition, the C-terminal 30 residues of CBP20 include Arg127, Gln133, and Val134, that directly contact the cap27.

To test whether the stabilization of the α2-α3 loop of CBP20 by Lys327 and Glu328 from CBP80 is important for high affinity cap-binding, we mutated these residues and assayed the ability of the CBC to be UV-cross-linked to [α^{32}P]GTP and capped-mRNA. While both the CBP80(K327A,E328A) double-mutant and wild-type CBP80 bound CBP20 equally well as determined by co-immunoprecipitation with HA-CBP20 from HeLa cells (Fig. 3b), the CBP80(K327A,E328A) double-mutant was unable to confer high affinity cap-binding to the CBP20 subunit, as indicated by its ineffective binding of either [α^{32}P]GTP or m^7GpppG-mRNA (Figs. 3c,d, respectively). Moreover, RNA gel-shift assays showed that deletion of the first 14 residues of CBP20, none of which directly contact the cap26,27 but are involved in binding to Lys327 and Glu328 of CBP80 (Fig. 3a inset), compromised the ability of CBP20 to bind the cap moiety (Fig. 3e, lane 6). Similarly, removal of the C-terminal 30 residues from CBP20 abrogated cap-binding activity (Fig. 3e, lane 7), as did the combined removal of the N-terminal 14 residues and the C-terminal 30 residues (Fig. 3e, lane 8).

Having established that residues 1–14 and 126–156 from CBP20 are required for high affinity cap-binding, we wanted to know if they are involved in the interaction with importin-β. Deletion of residues 1–14 from the N-terminus of CBP20, or residues 126–156 from the C-terminus, weakened but did not eliminate the binding of importin-β (Fig. 2b, compare lanes 1–4 with lanes 5–12), whereas the combined removal of the N- and C-terminal regions of CBP20 abolished CBP20-importin-β interactions (Fig. 2b, lanes 13–16). To ensure that the different CBP20 constructs were folded correctly we showed that each of the His-tagged CBP20 constructs was able to bind wild-type CBP80 as effectively as full-length CBP20 (Supplementary Fig. 5).

Structural model for the CBC-importin-α-importin-β complex

Given what we learned from the studies outlined in the preceding sections, we would predict that importin-β, when bound together with importin-α to the CBC, should be positioned near the CBP20 subunit. Therefore, we used small angle x-ray scattering (SAXS)30,31 in combination with the crystal structure information available for components of this complex and analytical ultracentrifugation experiments (AUC), to see whether structural models could be developed that were consistent with our biochemical findings.

Using the program BUNCH32, and the available structures for the CBC-importin-αΔIBB complex (Fig. 1), and the importin-β-importin-α-IBB domain complex (PDB ID 1QGK33), we added 25 "dummy residues" between Ser54 of importin-α within the importin-β-importin-α-IBB complex, and Asp79 of importin-α within the CBC-importin-αΔIBB complex, in order to connect the two crystallographic structures ("linker" in Fig. 4a). A portion of this stretch of residues within full-length importin-α forms a coiled-coil structure while the remainder of this segment is disordered21. Based on the length and stereo-chemical constraints of these additional residues, together with what we have learned regarding the contact regions between CBP20 and importin-β (see the preceding sections), the program was able to position importin-β in close contact with CBP20 and generate models for the CBC-importin-α-importin-β complex that were in good agreement with the experimental curve.

Figure 4a presents the best model obtained with BUNCH as judged by the χ value, while Fig. 4b shows the agreement of the experimental SAXS curve with the curve calculated for the best model. When we manually changed the position of importin-β by moving it away from its contact sites on the CBC, and then calculated the theoretical scattering curve and compared it to the experimental data by using CRYSOL34, this movement provoked a significant increase in the level of discrepancy between the theoretical curve and experimental data (Supplementary Fig. 6a). The SASREF32 program generated models that agreed with the BUNCH results (Supplementary Fig. 6b). The hydrodynamic ratio (R_H) and sedimentation values ($s_{20,w}$) from the best BUNCH model were calculated using HYDROPRO35 and compared to the same values obtained from sedimentation velocity AUC (Supplementary Fig. 7). The calculated values of 63.2 Å for R_H and 9.7 S for $s_{20,w}$ agree well with the experimental values of 65.0 Å and 9.5 S for R_H and $s_{20,w}$ respectively, providing further support for the model.

Based on these findings, together with our biochemical and mutagenesis data, as well as our structural work on the CBC-importin-α complex, we can propose a mechanistic model that describes how importin-β binds together with importin-α to the CBC and triggers the release of capped RNA (Fig. 4c). Within this model, the central portion of the importin-β molecule serves as a contact site for the N-terminal IBB domain of importin-α (Fig. 4a), enabling importin-β to form a complex with importin-α and the CBC. The region on importin-β containing residues 45–305 binds to the N-terminal 14 residues of the CBP20 subunit, displacing them from their contact site on CBP80 (Lys327 and Glu328). As we have shown, this contact stabilizes the α2-α3 loop of CBP20 and is essential for π-π interactions between Tyr20 and Tyr43 of CBP20 and the methylated guanosine ring of the cap moiety (Fig. 4c,

inset). Likewise, the binding of importin-β to the C-terminal region of CBP20, while not directly contacting Tyr138 of CBP20 (data not shown), most likely alters its position such that it no longer participates in a π-π stacking interaction with the second guanosine ring of the cap (Fig. 4c, inset). Together, these two interactions between importin-β and CBP20 would significantly weaken the affinity of CBP20 for capped RNA and thus promote its release from the CBC.

The importins regulate cap-binding to the CBC in cells

To verify that the importins regulate the cap-binding activity of the CBC in cells, as proposed in Fig. 4c, we took advantage of earlier findings that showed growth factors stimulate the incorporation of [α^{32}P]GTP into the cap-binding site of the CBP20 subunit36,37. In order for radiolabeled GTP to be incorporated into CBP20, RNA must first be released in the cytosol, prior to the nuclear import of the CBC, i.e. to form a pool of CBC that is RNA-depleted and available for [α^{32}P]GTP-incorporation. Therefore, if the binding of the importins to the CBC is necessary to trigger the release of cap (Fig. 4c), then this interaction should also be essential for growth factor-stimulated incorporation of [α^{32}P]GTP into CBP20. One way to test this would be to design an importin-β mutant that still binds to importin-α and the CBC, but is incapable of stimulating the dissociation of the cap, and then see if it blocks the growth factor-stimulated cap-binding activity of the CBC. However, changes made to importin-β such as limited deletions that affect its ability to regulate cap-binding also weaken its binding to importin-α. As an alternative strategy, we designed a CBP80 mutant that no longer binds through its N-terminal NLS to importin-α, but instead engages importin-α through an engineered stretch of NLS sequences at its C-terminus. Such a CBP80 mutant, when bound to endogenous CBP20, should yield a CBC that is incapable of a growth factor-stimulated incorporation of [α^{32}P]GTP, because of its inability to properly associate with the importins to release capped-RNA in the cytosol. The CBP80 mutant that we generated contained alanine residues in place of Lys17 and Arg18 within the NLS sequence. A triple NLS sequence (together with a V5-epitope) was attached to the C-terminus of the CBP80-double mutant, as well as to a control construct, to ensure that they would still undergo nuclear import (CBP80(K17A,R18A)-NLS and CBP80(WT-NLS), Fig. 5a). These proteins were transiently expressed in HeLa cells and visualized by immunofluorescence using an anti-V5 antibody. Figure 5b shows that unlike the CBP80(K17A,R18A) double-mutant, CBP80(K17A,R18A-NLS) was localized to the nucleus. CBP80(WT-NLS) and CBP80(K17A,R18A-NLS) were immunoprecipitated from nuclear lysates and shown to bind to HA-CBP20 equally well (Fig. 5c, bottom panel).

Cells transiently expressing either CBP80(WT-NLS) or CBP80(K17A,R18A-NLS) were then serum-starved and treated with or without heregulin, a growth factor which activates ErbB2 and is very effective in signaling to the CBC36,37. The CBP80 constructs were immunoprecipitated from nuclear extracts via their V5-tags and their associated CBP20 subunits were assayed for cap-binding by the incorporation of [α^{32}P]GTP. Only when the CBC was comprised of wild-type CBP20 and the CBP80(WT-NLS) protein, did it respond to heregulin with a marked increase in the incorporation of [α^{32}P]GTP (Fig. 5d). These findings demonstrate that the interactions of the importins with the CBC indeed influence its

cycle of capped RNA-binding and release, which is requisite for cap-dependent RNA-processing events.

DISCUSSION

The binding of capped RNA by eIF4E is necessary for the translation of mRNA into protein and is tightly regulated by growth factor-dependent signaling pathways1,38. Interestingly, the other major cap-binding complex in cells, the CBC, is also regulated by growth factors36,37, culminating in the directional binding of capped RNAs such that the CBC undergoes a high affinity interaction in the nucleus, but then releases the RNA in the cytosol. The fact that importin-β is a binding partner for Ran-GTP, and that Ran exists in the GTP-bound state in the nucleus but in the GDP-bound state in the cytosol, provide a mechanistic basis by which these changes in the cap-binding affinity of the CBC occur. In particular, the generation of Ran-GTP in the nucleus by the Ran-GEF RCC139 enables Ran to bind importin-β, which then causes importin-β to dissociate from the CBC-importin-α complex, ensuring that the CBC binds capped RNA with high affinity. It is not known if the CBC-capped RNA complex is exported from the nucleus together with, or independently of, importin-α, but its stable association with importin-α in the nucleus has been observed by us (data not shown) and others14-16. However, once in the cytosol, both importin-α and importin-β are able to bind to the CBC-capped-RNA complex, because Ran-GTP is converted to Ran-GDP by RanGAP and RanBP140,41, thereby allowing importin-β to dissociate from Ran and freeing it to engage (together with importin-α) the CBC-capped RNA complex and stimulate the dissociation of capped RNA. In the case of capped mRNA, this is a crucial step for the events leading to protein synthesis, whereas with U snRNAs, release from the CBC is necessary so that the cap may undergo cytoplasmic hypermethylation as part of the process of U snRNP maturation42,43. The CBC-importin-α-importin-β complex, depleted of capped RNA, is imported into the nucleus where importin-β will dissociate from the complex through its interaction with Ran-GTP, clearing the way for a new capped RNA molecule to bind to the CBC with high affinity. Recently, we found that the activation of Ran is regulated by growth factors (T. Ly, J. Wang, R. Pereira, X. Peng, Q. Feng, R. Cerione, K.F. Wilson, Cornell University, unpublished data), which likely explains how they stimulate the cap-binding capability of the CBC in the nucleus (Fig. 5d, also36,37).

Given the roles played by the importins in ensuring that the CBC binds capped RNA with the proper affinity at the right time and place in cells, we wanted to obtain a more detailed picture for how they bind to the CBC and confer their regulatory influences. Through a combination of structural and biochemical approaches, we discovered that importin-β is capable of directly binding to the CBP20 subunit through an interaction that requires the N- and C-terminal ends of CBP20, two regions that are necessary for the high affinity binding of capped-RNA. Our biochemical characterization of the CBP20-importin-β interaction, together with the available x-ray crystal structure for importin-β complexed to the importin-α-IBB domain and our recently solved structure for the CBC-importin-αΔIBB complex, as well as the data from SAXS experiments, now enable us to put forward a mechanistic picture that describes how importin-β, by interacting with importin-α through its IBB domain, can be properly positioned to engage the CBP20 subunit and weaken its affinity for

capped RNA (Fig. 4c). Moreover, we have been able to show that these interactions between the importins and the CBC are key steps in the growth factor-regulation of its cap-binding activity in cells. In the future, it will be interesting to see whether the interactions between the CBC and the importins might be directly regulated by extracellular signals. It also will be important to learn more about how the proper timing is established for the nucleocytoplasmic transport of the CBC, importin-α, and importin-β, so that the release of capped mRNA from the CBC can be coordinated with the regulation of eIF4E and RNA translation in the cytosol.

METHODS

Preparation of the CBC-importin-α and CBC-importin-α-importin-β complexes

Recombinant CBP20 and CBP80 co-expressed from insect cells were purified with the cap-analog m^7GpppG (New England BioLabs) as described27. Apo-CBC, comprised of CBP20 and CBP80 from insect cells (without tags), was purified by Q-Sepharose (GE Healthcare) chromatography followed by chromatography using Butyl Sepharose (GE Healthcare) and a Hiload Superdex 200 16/60 gel filtration column (GE Healthcare).

The cDNAs encoding full-length human importin-α isoform 1 (karyopherin-α2) and the N-terminal truncated importin-α construct lacking the first 69 amino acid residues (ΔIBB) were cloned into the pSUMO plasmid (LifeSensors, Malvern, PA). The C-terminal His-tagged importin-α construct used for crystallization was expressed from pET 30 (Invitrogen). The cDNAs encoding full-length human importin-β1 and the deletion mutant encoding residues 305–876 were cloned into pET28. The importin-β constructs encoding residues 1–619, 1–445, 45–876 (pTYB4 vector (NEB)) and 127–876 (pQE60 (Qiagen)) were kind gifts from Dr. Gino Cingolani (SUNY Upstate Medical University). The cDNAs encoding full-length CBP20 and the deletion mutants were inserted into pET28.

The purification of the His-tagged importin proteins, as well as His-tagged CBP20, were performed by IMAC (Immobilized metal affinity chromatography) using Co^{2+}-charged TALON resin (BD Biosciences), equilibrated with 30 mM Tris-HCl, pH 7.0, 300 mM NaCl, 0.3 mM TCEP (Tris(2-carboxyethyl)phosphine hydrochloride), and a cocktail of protease inhibitors. The proteins were eluted using this buffer plus 300 mM imidazole. The His-tags were removed using the appropriate cleavage enzyme. Purification of the pTYB4-cloned importin-β constructs involved the use of Chitin beads as described by the manufacturer (New England BioLabs).

The m^7GpppG-bound CBC-importin-α complex was prepared by combining m^7GTP-Sepharose (GE Healthcare)-purified CBC with IMAC-purified importin-α, followed by Mono-Q column (GE Healthcare) and Hiload Superdex 200 16/60 gel filtration column. The presence of m^7GpppG at equimolar concentrations was verified by analytical reverse-phase chromatography (Sunfire C-18 reverse-phase column (Waters)) in 100 mM phosphate buffer, pH 6.5, containing 10 mM tetra-butyl-ammonium bromide, 7.5% (v/v) acetonitrile, and 0.2 mM NaN3.

To prepare the apo-CBC-importin-α-importin-β complex, His-tagged CBP20 immobilized on Co^{2+}-charged TALON resin was used to pull-down CBP80 expressed in insect cells and purified using a Q-Sepharose column. His-tagged CBP20 plus CBP80 were then combined with importin-α and importin-β at equimolar concentrations and the resulting complex was eluted from the affinity column. Further purification was performed by Mono-Q chromatography followed by Hiload Superdex 200 L6/60 gel filtration chromatography.

Crystallization, x-ray data collection and processing

Crystals for the CBC-importin-α complex were obtained by using the hanging-drop vapor diffusion technique at 18°C from the following two conditions: 100 mM MES, pH 6.0, and 8% PEG 4000 (crystal 1); and, 100 mM Tris-HCl, pH 7.0, 12% PEG 8000, and 100 mM KCl (crystal 2). Diffraction data for crystal 1 was collected on an ADSC Q-315 detector (Area Detector Systems Corp.) at NE-CAT-24-ID-C (Advanced Photon Source (APS)) with λ = 0.97918 Å. The Cornell High Energy Synchrotron Source (CHESS) station F1 was used to collect the data set for crystal 2, using a Q-210 x-ray detector (λ = 0.91790 Å).

Drops were prepared by mixing equal parts of protein and the well solution, with the initial protein concentration being 10–20 mg ml^{-1}. Before data collection at cryogenic temperature (100 K), crystals were soaked in cryoprotectant solution containing the mother liquor prepared with 15% ethylene glycol. Data reduction was carried out with MOSFLM46, followed by SCALA47 and the HKL2000 package48 for crystals 1 and 2, respectively.

The space group for crystals 1 and 2 is $P12_11$. They also showed similar unit cell parameters. In both cases, the asymmetric unit consists of one molecule each of importin-α, CBP20, and CBP80. The cap-analog was absent in both crystal structures. The initial model for crystal 1 was obtained by molecular replacement using Phaser49 and human CBC (PDB ID 1N54, ref. 27) and mouse importin-α (1IAL21) as search molecules. For crystal 2, the program Molrep50 was employed using the higher resolution structure of the complex as a search molecule. Rigid-body refinement for crystal 1 followed by subsequent cycles of positional and B-factor refinements were carried out with Refmac51. Real space refinement through inspection of the Fourier electron density maps was performed with Coot52. Cycles of TLS were applied for crystal 1 as a final step of refinement. The model obtained from crystal 2 was refined with Phenix53. Solvent water molecules, treated as oxygen atoms, were added only to the crystal 1 model using the Coot routine52. The overall stereochemical quality of the final model, and the agreements between model and the experimental data, were assessed by both the program MolProbity54 and the proper Coot tools. Analysis of the Ramachandran plot showed 98% of the residues for the crystal 1 structure were within the preferred region, 1.6% within the allowed region and 0.4% as outliers. For crystal 2, the values were 91.5%, 7.1% and 1.4%, respectively.

SAXS data collection and rigid body modeling

SAXS data for the apo-CBC-importin-α-importin-β complex were collected at beamline 12-ID-C (BESSRC beamline) at APS. Scattering data were collected using protein concentrations of 2.5, 5 and 10 mg ml^{-1}, at a wavelength λ = 1.0332 Å, for sample-detector

distances of 0.4 m and 2 m covering the momentum transfer ranges $0.006 < s < 0.26$ Å^{-1}, and $0.017 < s < 0.62$ Å^{-1}, respectively ($s = 4\pi \sin\theta/\lambda$, where 2θ is the scattering angle).

The data were normalized to the intensity of the incident beam and corrected for the detector response using an in-house program. Five frames of 5 seconds were collected and compared for radiation damage using the program PRIMUS55. The same program was used to average the frames and subtract the buffer. The different protein concentrations were evaluated for aggregation by following increases in the measured *R*g (radius of gyration) as calculated by autoRg. As no changes were observed, the curve in Fig. 4b was obtained by merging the data collected for the 2.5 mg ml^{-1} sample at the long detector-sample distance with the data collected for the 10 mg ml^{-1} sample at the short distance. The *R*g was confirmed by using the indirect Fourier transform program GNOM44,45; this program was also used to calculate the distribution function $p(r)$ and *D*max.

Analytical ultracentrifugation sedimentation velocity experiments were performed to determine the molecular weight and homogeneity of the complex used for SAXS (see Supplementary Methods). The molecular weight was further confirmed by two approaches. The first used the dependence of the Krakty plot maximum position on the *R*g and the molecular weight for the case of a globular protein56 (the coordinates were generously provided to us by the authors). The second approach used the intensity $I(0)$ extrapolated for $s = 0$ for both the CBC-importin-α and CBC-importin-α-importin-β complexes.

The recently developed programs SASREF32 and BUNCH32 can be used such that the optimum position and orientation of the proteins comprising a complex are determined by minimizing the discrepancy between the experimental scattering data, and the theoretical scattering curve calculated from a structural model generated by using the x-ray structures of individual components. Using both programs the components of the tetramer (importin-β (PDB ID 1QGR33) and the CBC-importin-α complex) were treated as rigid-bodies and the modeling of domains to the SAXS data set was done through a simulated annealing protocol32, where discrepancy (between the experimental scattering data and the theoretical scattering curve calculated from the model) value is given by χ:

$$\chi^2 = \frac{1}{N-1}\sum_j \left[\frac{I_{exp}(S_j) - cI_{calc}(S_j)}{\sigma(S_j)}\right]^2,$$

where N is the number of experimental points, *c* is a scaling factor, $I_{exp}(S_j)$ and $I_{calc}(S_j)$ are the experimental and calculated intensities and $\sigma(S_j)$ is the experimental error at the momentum transfer S_j.

Two constraints were used, the distance between importin-α and its IBB domain crystallized with importin-β, and a contact between the region containing residues 45–305 from importin-β and CBP20. The program BUNCH was also used to find the probable conformation of the connection between residues 54 and 79 of importin-α by constructing a “dummy” atom chain. Five BUNCH32 and 5 SASREF32 simulations were computed and compared visually. CRYSOL34 was used to calculate the theoretical scattering curves for models where the subunits were manually positioned. HYDROPRO35 analysis of the best

BUNCH model used the number of values of the radius of the beads and the lowest and highest values of the radius as calculated by the program. The partial specific volume of the complex as well as the buffer density and viscosity were calculated by the program SEDNTERP57.

The reconstitution of good quality envelopes or low resolution bead models for the complex was not feasible due to its high molecular weight and inherent lack of symmetry.

Supplementary Material

Refer to Web version on PubMed Central for supplementary material.

Acknowledgments

This work was supported by NIH grant number GM40654. We would like to thank Dr. Gino Cingolani for assistance with the agarose-native gel assays and discussion of the results, Dr. Holger Sondermann and Qi Wang for helping with the APS data collection, Drs. Brian Crane, Mario Sanches, and Adriana Rojas for helpful discussions, and Cindy Westmiller for her excellent secretarial assistance. We also thank the CHESS and APS beamline staff for their assistance with the data collection.

References

1. von der Haar T, Gross JD, Wagner G, McCarthy JEG. The mRNA cap-binding protein eIF4E in post-transcriptional gene expression. Nat Struct Mol Biol. 2004; 11:503–511. [PubMed: 15164008]
2. Lewis JD, Izaurralde E. The role of the cap structure in RNA processing and nuclear export. Eur J Biochem. 1997; 247:461–469. [PubMed: 9266685]
3. Cheng H, et al. Human mRNA export machinery recruited to the 5’ end of mRNA. Cell. 2006; 127:1389–1400. [PubMed: 17190602]
4. Ishigaki Y, Li X, Serin G, Maquat LE. Evidence for a pioneer round of mRNA translation: mRNAs subject to nonsense-mediated decay in mammalian cells are bound by CBP80 and CBP20. Cell. 2001; 106:607–617. [PubMed: 11551508]
5. Lejeune F, Ishigaki Y, Li X, Maquat LE. The exon junction complex is detected on CBP80-bound but not eIF4E-bound mRNA in mammalian cells: dynamics of mRNP remodeling. EMBO J. 2002; 21:3536–3545. [PubMed: 12093754]
6. Maquat LE. Nonsense-mediated mRNA decay: splicing, translation and mRNP dynamics. Nat Rev Mol Cell Biol. 2004; 5:89–99. [PubMed: 15040442]
7. Ohno M, Segref A, Bachi A, Wilm M, Mattaj IW. PHAX, a mediator of U snRNA nuclear export whose activity is regulated by phosphorylation. Cell. 2000; 101:187–198. [PubMed: 10786834]
8. Segref A, Mattaj IW, Ohno M. The evolutionarily conserved region of the U snRNA export mediator PHAX is a novel RNA-binding domain that is essential for U snRNA export. RNA. 2001; 7:351–360. [PubMed: 11333016]
9. Flaherty SM, Fortes P, Izaurralde E, Mattaj IW, Gilmartin GM. Participation of the nuclear cap binding complex in pre-mRNA 3’ processing. Proc Natl Acad Sci USA. 1997; 94:11893–11898. [PubMed: 9342333]
10. Balatsos NA, Nilsson P, Mazza C, Cusack S, Virtanen A. Inhibition of mRNA deadenylation by the nuclear cap binding complex (CBC). J Biol Chem. 2006; 281:4517–4522. [PubMed: 16317009]
11. Fortes P, et al. The yeast nuclear cap binding complex can interact with translation factor eIF4G and mediate translation initiation. Mol Cell. 2000; 6:191–196. [PubMed: 10949040]
12. Izaurralde E, et al. A nuclear cap binding protein complex involved in pre-mRNA splicing. Cell. 1994; 78:657–668. [PubMed: 8069914]
13. Izaurralde E, McGuigan C, Mattaj IW. Nuclear localization of a cap-binding protein complex. Cold Spring Harb Symp Quant Biol. 1995; 60:669–675. [PubMed: 8824441]

14. Görlich D, et al. Importin provides a link between nuclear protein import and U snRNA export. Cell. 1996; 87:21–32. [PubMed: 8858145]
15. Li H, Tschudi C. Novel and essential subunits in the 300-kilodalton nuclear cap binding complex of. Mol Cell Biol. 2005; 25:2216–2226. [PubMed: 15743819]
16. Oeffinger M, et al. Comprehensive analysis of diverse ribonucleoprotein complexes. Nat Methods. 2007; 4:951–956. [PubMed: 17922018]
17. Wen Y, Shatkin AJ. Cap methyltransferase selective binding and methylation of GpppG-RNA are stimulated by importin-alpha. Genes Dev. 2000; 14:2944–2949. [PubMed: 11114884]
18. Görlich D, Panté N, Kutay U, Aebi U, Bischoff FR. Identification of different roles for RanGDP and RanGTP in nuclear protein import. EMBO J. 1996; 15:5584–5594. [PubMed: 8896452]
19. Tarendeau F, et al. Structure and nuclear import function of the C-terminal domain of influenza virus polymerase PB2 subunit. Nat Struct Mol Biol. 2007; 14:229–233. [PubMed: 17310249]
20. Conti E, Kuriyan J. Crystallographic analysis of the specific yet versatile recognition of distinct nuclear localization signals by karyopherin alpha. Structure. 2000; 8:329–338. [PubMed: 10745017]
21. Kobe B. Autoinhibition by an internal nuclear localization signal revealed by the crystal structure of mammalian importin alpha. Nat Struct Biol. 1999; 6:388–397. [PubMed: 10201409]
22. Conti E, Uy M, Leighton L, Blobel G, Kuriyan J. Crystallographic analysis of the recognition of a nuclear localization signal by the nuclear import factor karyopherin alpha. Cell. 1998; 94:193–204. [PubMed: 9695948]
23. Fontes MR, Teh T, Kobe B. Structural basis of recognition of monopartite and bipartite nuclear localization sequences by mammalian importin-alpha. J Mol Biol. 2000; 297:1183–1194. [PubMed: 10764582]
24. Fontes MR, Teh T, Jans D, Brinkworth RI, Kobe B. Structural basis for the specificity of bipartite nuclear localization sequence binding by importin-alpha. J Biol Chem. 2003; 278:27981–27987. [PubMed: 12695505]
25. Mazza C, Ohno M, Segref A, Mattaj IW, Cusack S. Crystal structure of the human nuclear cap binding complex. Mol Cell. 2001; 8:383–396. [PubMed: 11545740]
26. Mazza C, Segref A, Mattaj IW, Cusack S. Large-scale induced fit recognition of an m(7)GpppG cap analogue by the human nuclear cap-binding complex. EMBO J. 2002; 21:5548–5557. [PubMed: 12374755]
27. Calero G, et al. Structural basis of m7GpppG binding to the nuclear cap-binding protein complex. Nat Struct Biol. 2002; 9:912–917. [PubMed: 12434151]
28. Olia AS, et al. Binding-induced stabilization and assembly of the phage P22 tail accessory factor gp4. J Mol Biol. 2006; 363:558–576. [PubMed: 16970964]
29. Worch R, et al. Specificity of recognition of mRNA 5’ cap by human nuclear cap-binding complex. RNA. 2005; 11:1355–1363. [PubMed: 16043498]
30. Koch MH, Vachette P, Svergun DI. Small-angle scattering: a view on the properties, structures and structural changes of biological macromolecules in solution. Q Rev Biophys. 2003; 36:147–227. [PubMed: 14686102]
31. Putnam CD, Hammel M, Hura GL, Tainer JA. X-ray solution scattering (SAXS) combined with crystallography and computation: defining accurate macromolecular structures, conformations and assemblies in solution. Q Rev Biophys. 2007; 40:191–285. [PubMed: 18078545]
32. Petoukhov MV, Svergun DI. Global rigid body modeling of macromolecular complexes against small-angle scattering data. Biophys J. 2005; 89:1237–1250. [PubMed: 15923225]
33. Cingolani G, Petosa C, Weis K, Muller CW. Structure of importin-beta bound to the IBB domain of importin-alpha. Nature. 1999; 399:221–229. [PubMed: 10353244]
34. Svergun DI, Barberato C, Koch MHJ. CRYSOL – a program to evaluate x-ray solution scattering of biological macromolecules from atomic coordinates. J Appl Cryst. 1995; 28:768–773.
35. García De La Torre J, Huertas ML, Carrasco B. Calculation of hydrodynamic properties of globular proteins from their atomic-level structure. Biophys J. 2000; 78:719–730. [PubMed: 10653785]

36. Wilson KF, et al. The nuclear cap-binding complex is a novel target of growth factor receptor-coupled signal transduction. J Biol Chem. 1999; 274:4166–4173. [PubMed: 9933612]
37. Wilson KF, Wu WJ, Cerione RA. Cdc42 stimulates RNA splicing via the S6 kinase and a novel S6 kinase target, the nuclear cap-binding complex. J Biol Chem. 2000; 275:37307–37310. [PubMed: 10973943]
38. Mamane Y, et al. eIF4E-from translation to transformation. Oncogene. 2004; 23:3172–3179. [PubMed: 15094766]
39. Bischoff FR, Ponstingl H. Catalysis of guanine nucleotide exchange on Ran by the mitotic regulator RCC1. Nature. 1991; 354:80–82. [PubMed: 1944575]
40. Coutavas E, Ren M, Oppenheim JD, D'Eustachio P, Rush MG. Characterization of proteins that interact with the cell-cycle regulatory protein Ran/TC4. Nature. 1993; 366:585–587. [PubMed: 8255297]
41. Bischoff FR, Krebber H, Smirnova E, Dong W, Ponstingl H. Co-activation of RanGTPase and inhibition of GTP dissociation by Ran-GTP binding protein RanBP1. EMBO J. 1995; 14:705–715. [PubMed: 7882974]
42. Luhrmann R, Kastner B, Bach M. Structure of spliceosomal snRNPs and their role in pre-mRNA splicing. Biochim Biophys Acta. 1990; 1087:265–292. [PubMed: 2147394]
43. Izaurralde E, Mattaj IW. Transport of RNA between nucleus and cytoplasm. Semin Cell Biol. 1992; 3:279–288. [PubMed: 1384772]
44. Svergun DI. Mathematical methods in small-angle scattering data analysis. J Appl Cryst. 1991; 24:485–492.
45. Svergun DI. Determination of the regularization parameter in indirect-transform methods using perceptual criteria. J Appl Cryst. 1992; 25:495–503.
46. Leslie AGW. Recent changes to the MOSFLM package for processing film and image plate data. Joint CCP4 + ESF-EAMCB Newsletter on Protein Crystallography. 1992:26.
47. Evans, PR. Proceedings of CCP4 Study Weekend: Data Collection and Processing. Sawyer, L.; Isaacs, N.; Bailey, S., editors. Science and Engineering Research Council, Daresbury Laboratory; Warrington, United Kingdom: 1993. p. 114-122.
48. Otwinowski Z, Minor W. Processing of x-ray diffraction data collected in oscillation mode. Methods Enzymol. 1997; 276:307–326.
49. McCoy AJ, et al. Phaser crystallographic software. J Appl Cryst. 2007; 40:658–674. [PubMed: 19461840]
50. Vagin A, Teplyakov A. MOLREP: an automated program for molecular replacement. J Appl Cryst. 1997; 30:1022–1025.
51. Murshudov GN, Vagin AA, Dodson EJ. Refinement of macromolecular structures by the maximum-likelihood method. Acta Crystallogr D Biol Crystallogr. 1997; 53:240–255. [PubMed: 15299926]
52. Emsley P, Cowtan K. Coot: model-building tools for molecular graphics. Acta Crystallogr D Biol Crystallogr. 2004; 60:2126–2132. [PubMed: 15572765]
53. Adams PD, et al. PHENIX: building new software for automated crystallographic structure determination. Acta Cryst D Biol Crystallogr. 2002; 58:1948–1954. [PubMed: 12393927]
54. Davis IW, et al. MolProbity: all-atom contacts and structure validation for proteins and nucleic acids. Nucleic Acids Res. 2007; 35:W375–W383. [PubMed: 17452350]
55. Konarev PV, Volkov VV, Sokolova AV, Koch MHJ, Svergun DI. PRIMUS: a Windows PC-based system for small-angle scattering data analysis. J Appl Cryst. 2003; 36:1277–1282.
56. Semisotnov GV, Timchenko AA, Melnik BS, Kimura K, Kihara H. Kratky plot as a tool to evaluate the molecular mass of globular proteins. Photon Factory Activity Report 2002. 2003; 20(Part B):256.
57. Laue, TM.; Shah, BD.; Ridgeway, TM.; Pelletier, SL. Computer-aided interpretation of analytical sedimentation data for proteins. In: Harding, SE.; Rowe, AJ.; Horton, JC., editors. Analytical Ultracentrifugation in Biochemistry and Polymer Science. Royal Society of Chemistry; Cambridge, United Kingdom: 1992. p. 90-125.

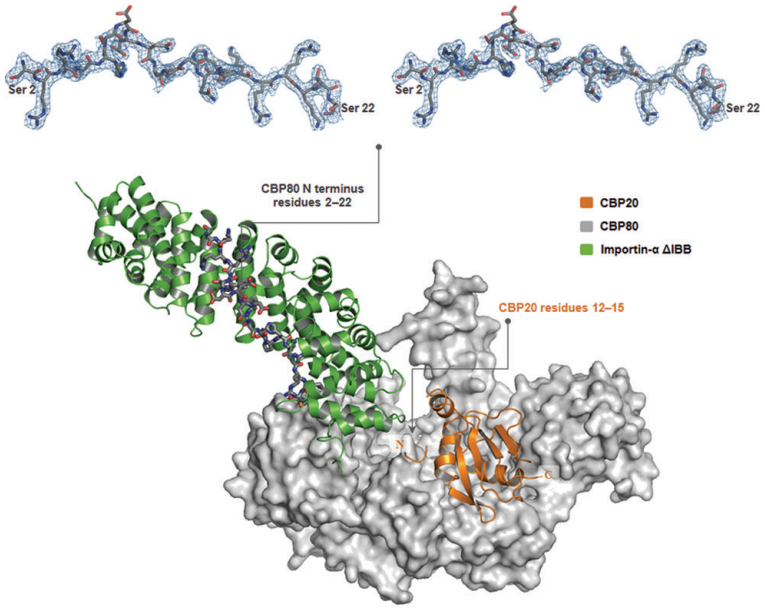

Figure 1.

Structural analyses of the CBC-importin-α complex. X-ray crystal structure of the CBC-importin-αΔIBB complex. CBP80 is shown as a surface (gray), while CBP20 and importin-α are depicted by ribbon diagrams (orange and green, respectively). Also shown is the N-terminal region of CBP80, residues 2 to 22 (represented by sticks), which contains the NLS segment of this protein along with its electron density map $2F_o-F_c$ countered at σ level 1 (inset sterio view).

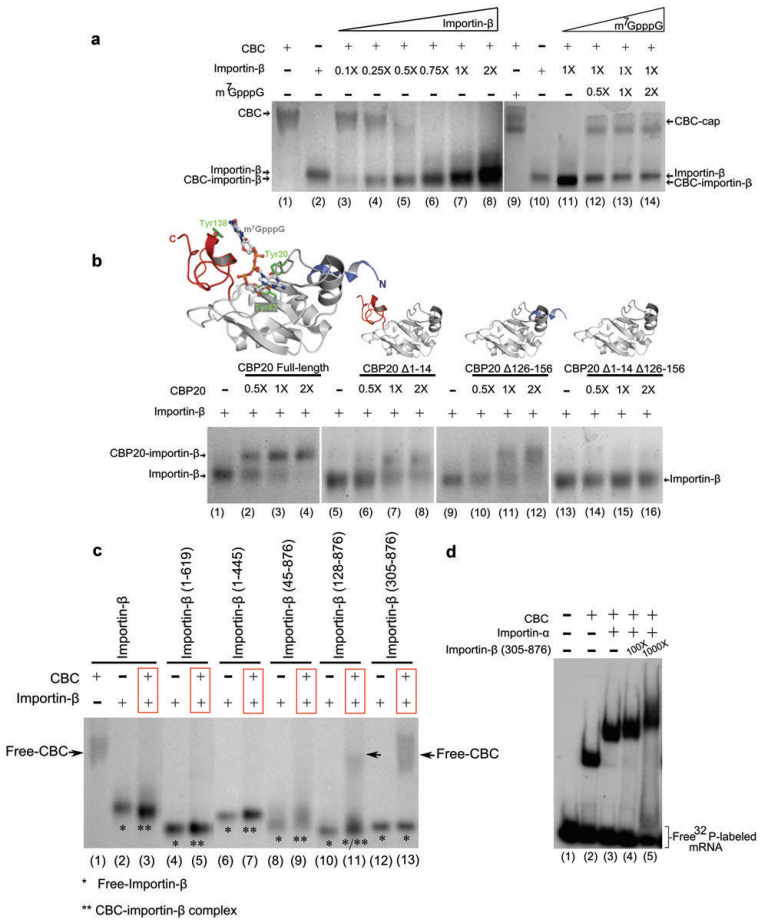

Figure 2.

Interaction of importin-β with the CBC. (**a**) Native gel electrophoresis of the CBC (lane 1), importin-β (lane 2), and the CBC pre-incubated with increasing amounts of importin-β (lanes 3 to 8), with a 10-fold molar excess of m^7GpppG (lane 9), and with importin-β and increasing amounts of m^7GpppG (lanes 11 to 14). Lanes 1–8, 1X Bis-Tris-running buffer; 9–14, 1X Tris-Glycine. (**b**) Native gel electrophoresis in 1X Bis-Tris buffer of importin-β (lanes 1, 5, 9 and 13), and importin-β pre-incubated with increasing amounts of full-length CBP20 (lanes 2 to 4), and different CBP20 constructs (lanes 6 to 16). The crystallographic structures of full-length CBP20 bound to cap (PDB ID 1N52, ref. 27) and the CBP20 deletion mutants are shown. (**c**) Native gel electrophoresis in 1X Bis-Tris buffer of the CBC (lane 1), full-length importin-β alone (lane 2), or pre-incubated with equimolar CBC (lane 3). The same was repeated with the following importin-β deletion mutants: importin-β (residues 1–619) (lanes 4 and 5), importin-β (residues 1–445) (lanes 6 and 7), importin-β (residues 45–876) (lanes 8 and 9), importin-β (residues 128–876) (lanes 10 and 11), and importin-β (residues 304–876) (lanes 12 and 13). (**d**) Electrophoretic mobility shift assays of the binding of ^{32}P-labeled capped mRNA to the CBC alone (lane 2), incubated with importin-α (lane 3), or incubated with equimolar importin-α and importin-β (residues 305–876) at an 100X (lane 4) or 1000X (lane 5) excess over the CBC.

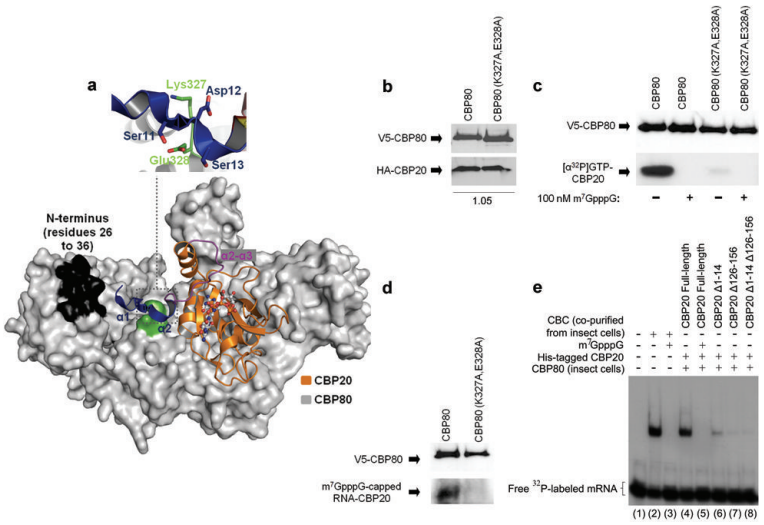

Figure 3.

Interactions between the N-terminus of CBP20 and its binding groove within CBP80. (**a**) Surface (CBP80) and ribbon (CBP20) representations of the CBC (PDB ID 1N52, ref. 27) illustrate the stabilization of the N-terminal hinge of CBP20 by residues in its binding groove within CBP80. The N-terminal region of CBP20 (that includes residues Ser11, Asp12, and Ser13, shown in dark blue) enters a groove formed by residues Lys327 and Glu328 of CBP80 (green), making contacts that stabilize residues of CBP20 in loop α2-α3 (magenta) in the cap-bound conformation. The inset shows these interactions in detail. Residues 26 to 36 of the N-terminal region of CBP80 are in black. (**b**) HeLa cells were transiently transfected with constructs encoding V5-CBP80 or V5-CBP80(K327A,E328A) and HA-CBP20 as indicated for 24 h. The expressed CBP80 proteins were immunoprecipitated with anti-V5 and Western blotted with anti-HA to show that CBP20 co-imunoprecipitated equally well with wild-type and mutated CBP80 (as quantified by densitometry). Immunoprecipitated CBC was assayed for UV-crosslinking incorporation of [α^{32}P]GTP (**c**) and ^{32}P-labeled capped-mRNA (**d**), with and without an excess of cap. (**e**) Electrophoretic mobility shift assays of ^{32}P-labeled capped mRNA incubated with the CBC alone (lane 2), CBC plus 100 μM m^{7}GpppG (lane 3), CBP80 plus full-length CBP20 without (lane 4) and with 100μM m^{7}GpppG (lane 5), and CBP80 plus either CBP20 Δ1–14 (lane 6), CBP20 Δ126–156 (lane 7) or CBP20 Δ1–14Δ126–156 (lane 8).

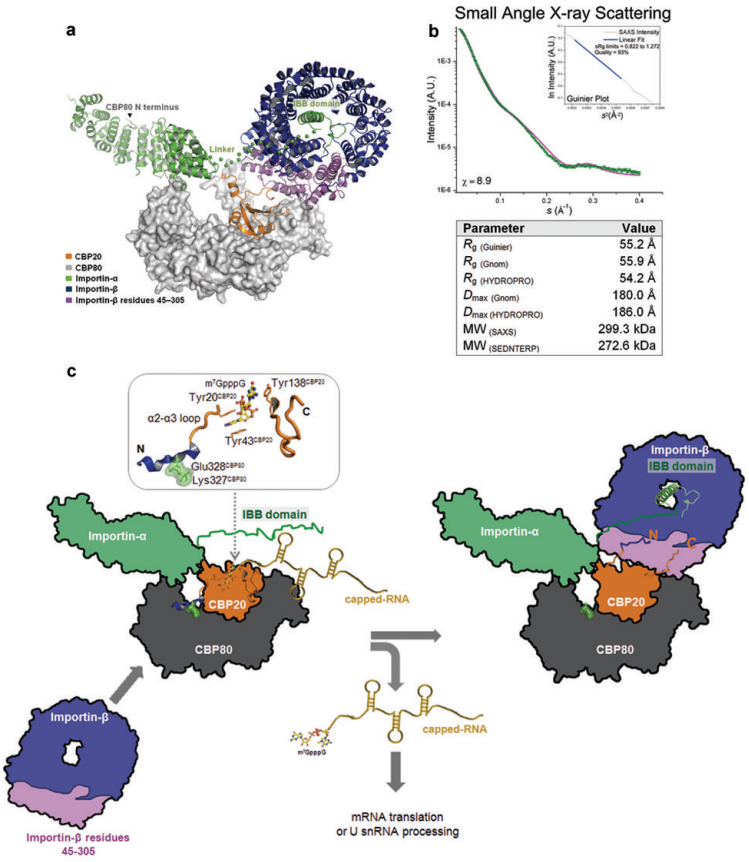

Figure 4.

Structural model for the CBC-importin-α-importin-β complex. (**a**) Modeling of the CBC-importin-α-importin-β complex was performed using the program BUNCH32 and the crystallographic structures of the CBC-importin-α complex, with CBP80 as a gray surface, CBP20 in orange ribbon, and importin-β in blue ribbon (PDB ID 1QGR33). (**b**) The superposition of the calculated scattering curve (magenta) of the best model obtained by BUNCH and the experimental SAXS curve (green with error bars). Below the graphic are the values for the radius of gyration, obtained by the Guinier approximation ($Rg_{(Guinier)}$; also, see inset, calculated with AutoRg) and calculated from real space by the program GNOM44,45 ($Rg_{(Gnom)}$). The values are comparable to the *R*g calculated from the model using HYDROPRO35 ($Rg_{(HYDROPRO)}$). Also shown are the D_{max} obtained from the program GNOM ($D_{max\ (Gnom)}$) calculated $p(r)$ and the value calculated from the model using HYDROPRO ($D_{max\ (HYDROPRO)}$). *R*g value calculated from the model is slightly smaller than the experimental values due to the fact that the model was built using the incomplete x-ray crystallographic structures of all four proteins. (**c**) Model for importin-β-mediated release of cap. The CBC-capped-RNA-importin-α complex engages importin-β in the cytosol, which has dissociated from Ran due to GTP hydrolysis. Importin-β binds to this complex through its interactions with the IBB domain of importin-α and the N- and C-terminal ends of the CBP20 subunit, which triggers the dissociation of capped mRNA as explained in the main text.

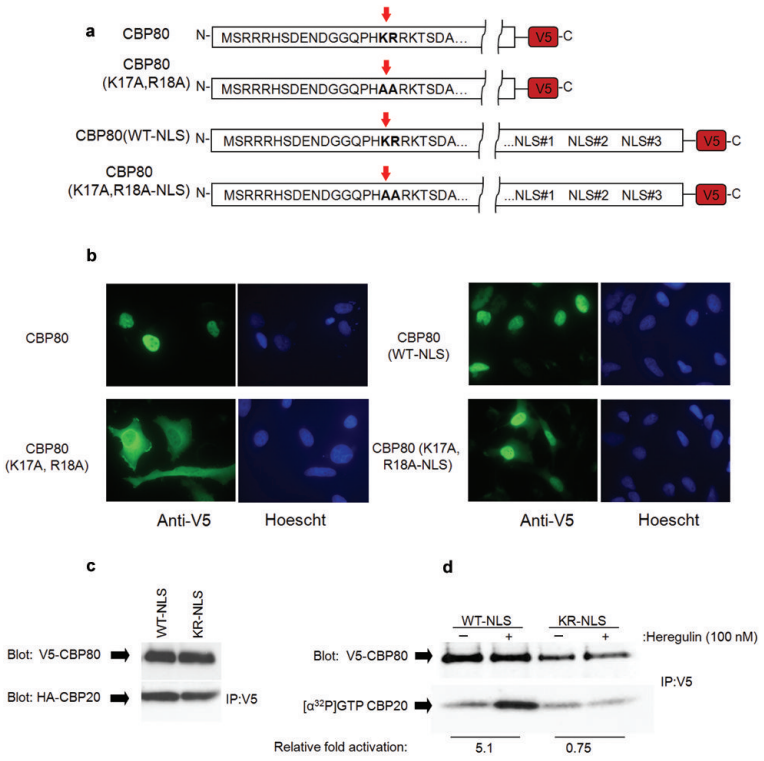

Figure 5.

Binding of importin-α to the N-terminus of CBP80 is necessary for growth factor-mediated changes in cap-binding by the CBC. (**a**) Schematic diagrams depicting the different CBP80 constructs used in these studies. (**b**) HeLa cells were transiently transfected with different V5-tagged CBP80 constructs for 24 h. Immunofluorescence was then performed to detect the localization of the expressed proteins using an anti-V5 antibody, and nuclear localization by Hoescht stain. (**c**) HeLa cells were transiently transfected with V5-tagged CBP80 and HA-CBP20 for 24 h. CBP80 constructs were immunoprecipitated and then subjected to SDS-PAGE and Western blotting to assess complex formation between the different CBP80 constructs (top panel) and HA-CBP20 (bottom panel). (**d**) HeLa cells were transiently transfected with CBP80 constructs, serum-starved for 48 h, and then stimulated with (+) or without (−) 100 nM heregulin for an additional 24 h. The CBC was immunoprecipitated and the isolated CBC complexes were assayed for [α^{32}P]GTP incorporation into CBP20. The top panel is a Western blot detecting the immunopreciptated V5-CBP80 proteins, and the bottom panel shows the incorporation of [α^{32}P]GTP into the cap-binding site of CBP20. Quantitation was performed by densitometry. Relative fold activation was determined by comparing the number of pixels measured for the unstimulated and stimulated incorporation of [α^{32}P]GTP. The results are representative of three individual experiments.

Table 1

Data collection and refinement statistics

	Crystal 1[a]	Crystal 2[a]
Data collection		
Space group	$P2_1$	$P2_1$
Cell dimensions		
a, *b*, *c* (Å)	83.84, 104.50, 108.56	83.50, 102.05, 107.88
α, β, γ (°)	90.00, 109.04, 90.00	90.00, 108.8, 90.00
Resolution (Å)	2.20 (2.32 – 2.20)[b]	3.50 (3.62 – 3.50)
R_{sym}	0.08 (0.57)	0.16 (0.43)
$I / \sigma I$	12.0 (2.0)	6.0 (2.6)
Completeness (%)	97.2 (83.6)	91.4 (92.5)
Redundancy	4.5 (3.7)	2.9 (2.9)
Refinement		
Resolution (Å)	15.00 – 2.20[b]	15.65 – 3.55
No. reflections	82,641	18,063
R_{work} / R_{free}	19.16/23.80	21.7/29.2
No. atoms		
Protein	10,292	10,050
Water	454	No water added
B-factors		
Protein	22.80	70.00
Water	29.78	No water added
R.m.s. deviations		
Bond lengths (Å)	0.011	0.005
Bond angles (°)	1.249	0.549

[a] A single crystal was used for each structure.

[b] Values in parentheses are for highest-resolution shell.